Toward Deciphering the Code to Aminergic G Protein-Coupled Receptor Drug Design

Edwin S. Tan,[1,5] Eli S. Groban,[2] Matthew P. Jacobson,[3] and Thomas S. Scanlan[4,*]
[1]Chemistry and Chemical Biology Graduate Program
[2]Graduate Group in Biophysics
[3]Department of Pharmaceutical Chemistry
University of California, San Francisco, San Francisco, CA 94158, USA
[4]Department of Physiology and Pharmacology, Oregon Health and Science University, Portland, OR 97239, USA
[5]Present address: Department of Systems Biology, Harvard Medical School, 200 Longwood Avenue, WA 536, Boston, MA 02115, USA.
*Correspondence: scanlant@ohsu.edu
DOI 10.1016/j.chembiol.2008.03.004

SUMMARY

The trace amine-associated receptor 1 ($TAAR_1$) is a biogenic amine G protein-coupled receptor (GPCR) that is potently activated by 3-iodothyronamine (1, T_1AM) in vitro. Compound 1 is an endogenous derivative of the thyroid hormone thyroxine which rapidly induces hypothermia, anergia, and bradycardia when administered to mice. To explore the role of $TAAR_1$ in mediating the effects of 1, we rationally designed and synthesized rat $TAAR_1$ superagonists and lead antagonists using the rotamer toggle switch model of aminergic GPCR activation. The functional activity of a ligand is proposed to be correlated to its probable interactions with the rotamer switch residues; agonists allow the rotamer switch residues to toggle to their active conformation, whereas antagonists interfere with this conformational transition. These agonist and antagonist design principles provide a conceptual model for understanding the relationship between the molecular structure of a drug and its pharmacological properties.

INTRODUCTION

3-iodothyronamine (**1**, T_1AM; Figure 1A) is an endogenous, decarboxylated, and deiodinated metabolite of the thyroid hormone thyroxine (T_4; Figure 1A) that is found in the brain, heart, liver, and blood (Scanlan et al., 2004). When administered to mice intraperitoneally, **1** rapidly induces hypothermia, anergia, and bradycardia, effects of which are opposite those observed with hyperthyroidism. In vitro, **1** induces the production of cAMP (adenosine 3′,5′-cyclic monophosphate) in HEK293 (human embryonic kidney 293) cells stably transfected with the G protein-coupled receptor (GPCR) known as $TAAR_1$ (Hart et al., 2006; Scanlan et al., 2004; Wainscott et al., 2007; Zucchi et al., 2006). Additionally, **1** has been found to inhibit neurotransmitter reuptake by the dopamine (DAT) and norepinephrine transporter (NET), and inhibits vesicular packaging by the vesicular monoamine transporter 2 (VMAT2) (Snead et al., 2007). To understand the role of $TAAR_1$ in mediating the effects of **1**, we sought to develop small molecules that regulate the activity of $TAAR_1$.

Rat $TAAR_1$ ($rTAAR_1$) is homologous to the β_2 adrenergic (β_2AR), dopamine, and serotonin receptors and belongs to the biogenic amine subfamily of class A rhodopsin-like GPCRs (Borowsky et al., 2001; Bunzow et al., 2001; Lindemann et al., 2005). GPCRs are seven-transmembrane (TM) proteins with an extracellular amino terminus and an intracellular carboxy terminus (Figures 1B and 1C; Gether, 2000; Wess, 1998). The binding site of aminergic GPCRs is located within the TM region and is primarily composed of the extracellular half of transmembranes 3, 5, 6, and 7 (Cherezov et al., 2007; Rasmussen et al., 2007; Rosenbaum et al., 2007; Tota et al., 1991). Elegant pharmacological and mutagenesis studies on β_2AR suggest that epinephrine binds to β_2AR with aspartic acid 3.32 (D3.32) acting as the counterion for the charged amine, serine residues 5.42, 5.43, and 5.46 (S5.42, S5.43, and S5.46, respectively) interacting with the catechol hydroxyls, phenylalanines 6.51 and 6.52 (F6.51 and F6.52) interacting with the catechol ring, and asparagine 6.55 (N6.55) as the partner for the β-hydroxyl group (Figure 1D) (see Experimental Procedures for a description of the residue indexing system) (Liapakis et al., 2000; Shi and Javitch, 2002; Strader et al., 1988, 1989a, 1989b, 1994; Wieland et al., 1996; Zuurmond et al., 1999).

Previous work with the β_2AR suggests that agonist binding toggles a rotamer switch to its active configuration and induces a conformational change in TM6 (Figure 2; Shi et al., 2002). The movement of the cytoplasmic end of TM6 away from TM3 is thought to break an ionic lock interaction that is present in the inactive state of the receptor (Figure 2A). This exposes G protein recognition sites in the intracellular surface of the receptor that activate G proteins and initiate the signaling cascade (Ballesteros et al., 2001; Yao et al., 2006). The rotamer switch is partly composed of tryptophan (W6.48) and phenylalanine (F6.52) residues in TM6 that toggle concertedly between their inactive (Figure 2A) and active (Figure 2B) rotamer configurations to modulate the bend angle of the kink in TM6 formed by proline 6.50 (P6.50). The ionic lock involves highly conserved aspartic acid (D3.49) and arginine (R3.50) residues in TM3 and a glutamic acid (E6.30) residue in TM6. The absolute conservation of the rotamer switch and ionic lock residues in $rTAAR_1$ suggests a mechanism of activation for $rTAAR_1$ similar to β_2AR.

Studies probing the mechanism of agonist-induced conformational changes in the β_2AR have found that agonist binding

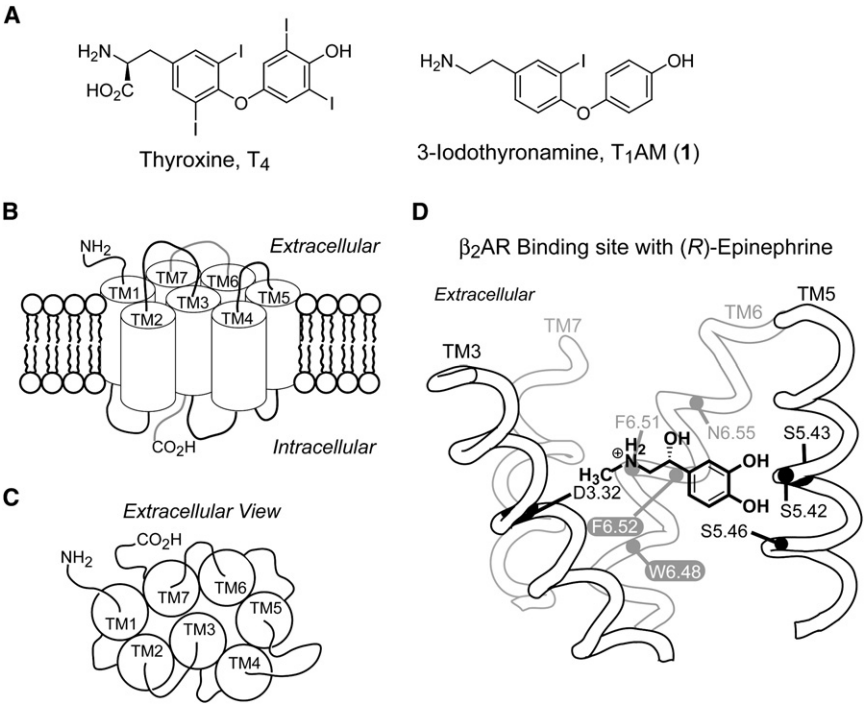

Figure 1. Hormones, Metabolites, and Biogenic Amine GPCR

(A) Structures of thyroxine (T_4) and 3-iodothyronamine (**1**, T_1AM).

(B and C) Schematic representations of the helical arrangement of GPCRs viewed from the cell membrane (B) and extracellular surface (C).

(D) Binding orientation of (*R*)-epinephrine in the binding site of the β_2AR viewed from the perspective of TM4. The locations of the rotamer switch residues (white letters) (see Figure 2) and residues known to interact with (*R*)-epinephrine are labeled. The residue indexing system is described in the Experimental Procedures.

occurs in a sequential process involving a series of conformational intermediates that have increasing numbers of interactions with the agonist as the receptor moves toward the fully active state (Kobilka and Deupi, 2007). The binding site of β_2AR is not prearranged to simultaneously interact with all of the functional groups of a given agonist like epinephrine (Figure 1D). Upon binding, only a few structural elements of epinephrine (i.e., the amine and catechol moiety) are proposed to be engaged with the β_2AR. These initial interactions induce a conformation transition to an intermediate that reveals additional contact points that interact with the β-hydroxyl and/or N-methyl groups. The functional groups of epinephrine have a synergistic effect on binding affinity and receptor activation and collectively influence the overall conformation of the active receptor (Liapakis et al., 2004). The ensemble of active receptor states induced by different agonists may have disparate functional properties and have different capacities to activate downstream effector molecules such as G_s protein, GPCR receptor kinase, and/or arrestin (Swaminath et al., 2004).

Despite being a major drug target and having insights into the molecular mechanism of GPCR activation and agonist-induced conformational changes, the nature of the ligand-receptor interaction is not fully understood. Although there have been many successful campaigns into GPCR drug design, it is surprising to find that there are no general postulates that can serve as guiding principles in the process of agonist and/or antagonist

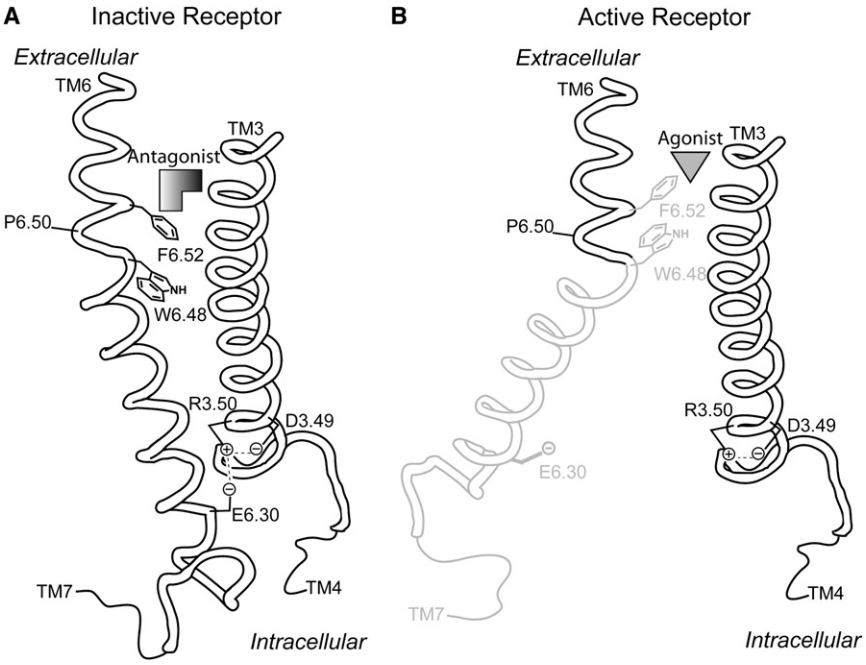

Figure 2. Rotamer Toggle Switch Model of Aminergic GPCR Activation

(A) Inactive state of the receptor with an antagonist sterically occluding the rotamer switch residues (W6.48 and F6.52) from assuming their active conformation.

(B) Agonist binding toggles the rotamer switch to its active conformation and induces a conformational change in TM6 that breaks the ionic lock interaction (D3.49, R3.50, and E6.30) present in the inactive state of the receptor.

(A) and (B) are viewed from the perspective of TM7; see Figures 1B and 1C.

development without requiring extensive structure-activity relationship (SAR) data to develop a pharmacophore for the receptor of interest. Even with pharmacophore models in hand, the code to aminergic GPCR drug design is still unknown. Presently, it is unclear what inherent structural features of a ligand are responsible for endowing agonistic or antagonistic properties or how and why those structural elements lead to receptor activation or inhibition.

Based on the rotamer toggle switch model, we hypothesized that the functional properties of a compound are determined by the nature of its interaction with the rotamer switch residues. If a compound allows the rotamer switch to toggle and/or has more favorable interactions with the active state of the receptor, it will act as an agonist (Figure 2B). In contrast, a compound will behave as an antagonist if it can sterically occlude the rotamer switch and/or has more favorable interactions with the inactive state of the receptor (Figure 2A). Herein we describe the rational design and synthesis of $rTAAR_1$ superagonists (agonists that are more potent and/or more efficacious than **1**) and lead antagonists guided by the rotamer toggle switch model of aminergic GPCR activation.

RESULTS

Development of $rTAAR_1$ Superagonists

The ligand binding site of $rTAAR_1$ differs from that of the β_2AR in that two hydrophobic residues, alanine (A5.42) and phenylalanine (F5.43) (Figure 3B), replace the serine residues S5.42 and S5.43 in TM5 (Figure 1D). By analogy to the catecholamines (epinephrine, norepinephrine, and dopamine), we speculate that **2** (Figure 3A; Tan et al., 2007), a potent $rTAAR_1$ agonist, is anchored into the binding site by the salt bridge interaction between the charged amine and D3.32, and the hydrogen bond interaction between the biaryl ether oxygen and S5.46 (Figure 3B). To experimentally test this hypothesis, a series of derivatives of **2** containing functional groups at the β-phenyl ring (ring C in Figure 3A) was synthesized. We specifically incorporated polar functional groups (**3**–**7**) (Table 1) capable of forming hydrogen bond interactions because our homology model of $rTAAR_1$ (see the Experimental Procedures for a description of how the model was generated), which was based on the crystal structure of bovine rhodopsin, showed that the surrounding residues around the β-phenyl ring would be asparagines (N7.35 and N7.39), a methionine (M6.55), and a cysteine (C6.54) (Figure 3B). Therefore, if **2** binds in this orientation, having functional groups that can interact with these residues should theoretically enhance binding affinity and thus increase potency. Additionally, fluorine-substituted analogs of **2** (**8** and **9**) (Table 1) were also synthesized to determine the effects of decreasing the electron density of the β-phenyl ring on $rTAAR_1$ activation. Compounds **3**–**9** were synthesized from 4-bromodiphenylether and a mono-substituted benzaldehyde in four to seven steps (see Supplemental Schemes 1 and 2 in the Suplemental Data available with this article online). Detailed synthetic procedures for compounds **2**–**56** are described in the Supplemental Data.

In HEK293 stable cell lines, **2** (EC_{50} = 28 ± 2 nM, E_{max} = 103 ± 4%) activates the stimulatory G protein-coupled $rTAAR_1$ at the same level as **1** (EC_{50} = 33 ± 3 nM, E_{max} = 100% ± 0%) (Table 1) (Tan et al., 2007). Representative dose-response curves of agonists for $rTAAR_1$ are shown in Figure S1A. Appending a methoxy group at the *para* (**3**) or *ortho* (**4**) position of the β-phenyl ring in **2** was detrimental, decreasing the potency ~5- to 6-fold and the efficacy 19%–35% (**3**, EC_{50} = 142 ± 40 nM, E_{max} = 68% ± 8%, and **4**, EC_{50} = 163 ± 18 nM, E_{max} = 84% ± 2%) (Table 1). A hydroxyl group at the β-phenyl ring was well tolerated by $rTAAR_1$ but only at the *para* position. The potency of the *para*-hydroxyl derivative **5** increased ~4.5-fold (EC_{50} = 6 ± 1 nM) and its efficacy was slightly enhanced (E_{max} = 114% ± 9%). When the hydroxyl substituent was located at the *ortho* (**6**) or *meta* (**7**) position, the potency decreased ~7.5- to 16.5-fold (EC_{50} = 467 ± 107 nM and 212 ± 39 nM, respectively), whereas the efficacy either decreased or was unaffected (E_{max} = 70% ± 6% and 106% ± 7%, respectively). Similarly, $rTAAR_1$ somewhat prefers a fluorine group at the *para* over the *meta* position, as the potency was the same for **8** (EC_{50} = 28 ± 6 nM) but decreased 2-fold for **9** (EC_{50} = 57 ± 6 nM). The efficacies of **8** and **9** (E_{max} = 99% ± 9% and 110% ± 2%, respectively) were unaffected by fluorination and were similar to that of **2**. All compounds with stereogenic centers (**2**–**50** and **52**–**56**) were evaluated as racemic mixtures. The observed activities of all compounds tested (**1**–**56**) were found to be $rTAAR_1$ dependent, as all compounds showed no cAMP accumulation when exposed to an empty vector control cell line (data not shown).

In an effort to improve the potency of **5**, we explored its tolerance for methylation at the amine, iodination of the inner ring, and hydroxylation of the outer ring. These modifications, individually or in combination, have previously been found to be beneficial for $rTAAR_1$ activation (Hart et al., 2006). Mono-methylation of the amine in **5** provided **10**, whereas mono-iodination of the inner ring yielded **11** (Supplemental Schemes 3 and 4). Adding a hydroxyl group to the *para* or *meta* position of the outer ring in **11** gave **12** and **13**, respectively (Supplemental Scheme 4).

When screened for agonist activity, some of the **5** derivatives were more efficacious but none were more potent. N-methylation of **5** (**10**) was beneficial, increasing the efficacy 13% (E_{max} = 127% ± 2%), but it did not improve potency (EC_{50} = 5 ± 1 nM) (Table 1). Mono-iodination of the inner ring (**11**) was unfavorable, decreasing potency ~3-fold (EC_{50} = 17 ± 2 nM) without significantly affecting efficacy (E_{max} = 107% ± 8%). In the presence of an outer ring *para*-hydroxyl group (**12**), the $rTAAR_1$ activity improved back to the level of **5** (EC_{50} = 4 ± 1 nM, E_{max} = 115% ± 2%). In contrast, a *meta*-hydroxyl group on the outer ring of **11** (**13**) had no effect on potency and efficacy (EC_{50} = 22 ± 2 nM and E_{max} = 111% ± 9%).

Development of $rTAAR_1$ Lead Antagonist

According to our proposed binding orientation of **2** in $rTAAR_1$ (Figure 3B), the rotamer switch residues are located in the vicinity of position 2 of the inner ring (ring B in Figure 3A). Using the toggle switch model of aminergic GPCR activation as a guideline (Figure 2), we attempted to convert **2** into an antagonist by appending functional groups at the 2 position to theoretically interfere with the rotamer switch residues. An alcohol group was installed into the 2 position (R_5; Table 2) of **2** (**14**) to serve as a handle for synthesizing a panel of ethers (**15**–**24**) and esters (**25** and **26**) varying in steric bulk, rigidity, topology, and polarity (Table 2; Supplemental Schemes 5 and 6).

The effects of the ether and ester substituents on receptor agonist activity were variable. The core scaffold **14** and ethyl ether **16** were decent agonists, activating to the same efficacy level as

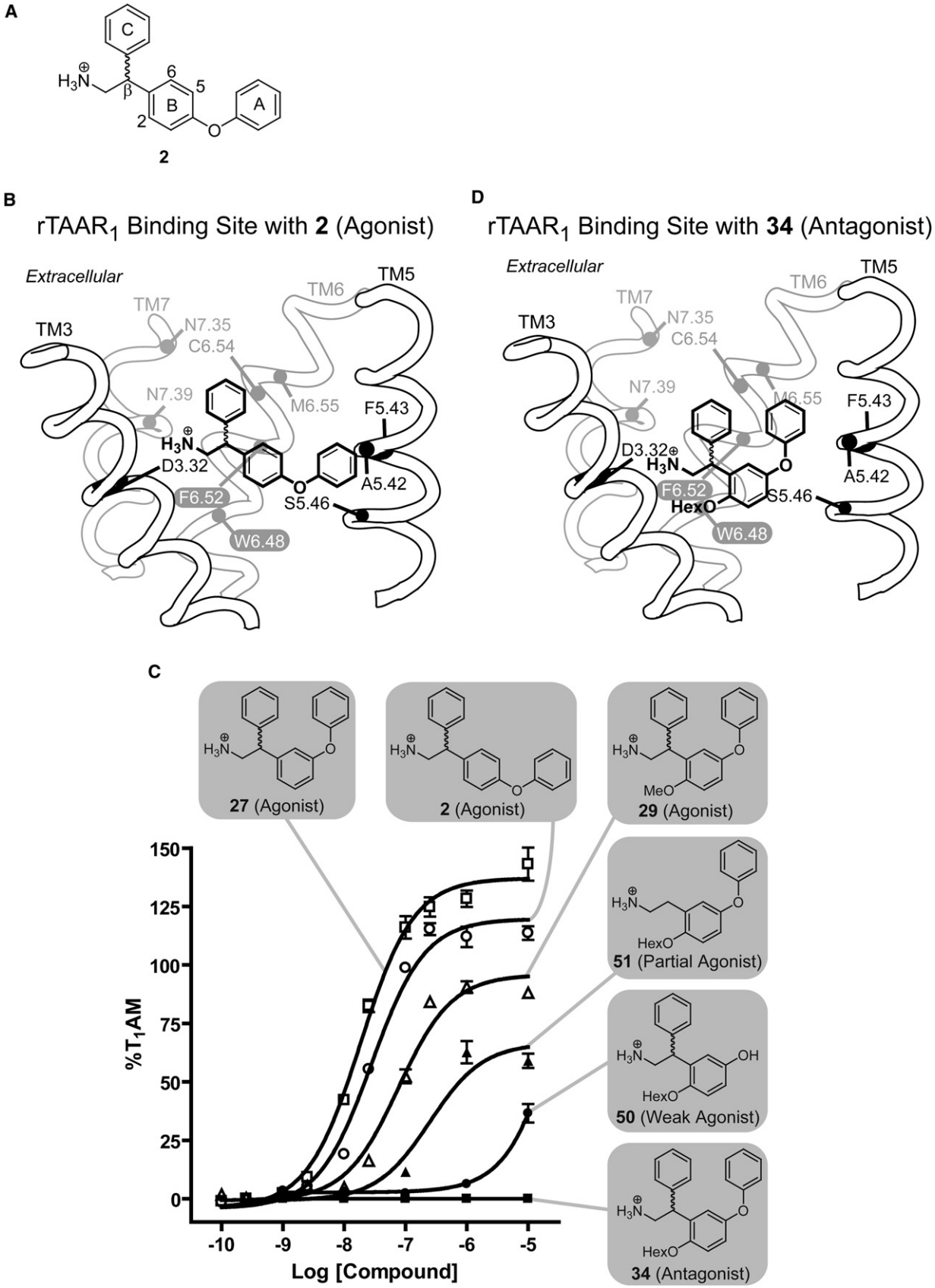

Table 1. Agonist Activity of Compounds 1–13 on rTAAR$_1$

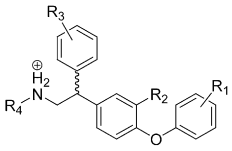

Compound	R_1	R_2	R_3	R_4	EC_{50}[a] ± SEM (nM)	E_{max}[b] ± SEM (%)	N[c]
1 (T_1AM)	see Figure 1				33 ± 3	100 ± 0	5
2 (ET-13)	H	H	H	H	28 ± 2	103 ± 4	3
3 (ET-34)	H	H	*p*-OMe	H	142 ± 40	68 ± 8	3
4 (ET-35)	H	H	*o*-OMe	H	163 ± 18	84 ± 2	3
5 (ET-36)	H	H	*p*-OH	H	6 ± 1	114 ± 9	4
6 (ET-37)	H	H	*o*-OH	H	467 ± 107	70 ± 6	3
7 (ET-65)	H	H	*m*-OH	H	212 ± 39	106 ± 7	3
8 (ET-66)	H	H	*p*-F	H	28 ± 6	99 ± 9	3
9 (ET-67)	H	H	*m*-F	H	57 ± 6	110 ± 7	3
10 (ET-64)	H	H	*p*-OH	Me	5 ± 1	127 ± 2	4
11 (ET-68)	H	I	*p*-OH	H	17 ± 2	107 ± 8	4
12 (ET-69)	*p*-OH	I	*p*-OH	H	4 ± 1	115 ± 2	6
13 (ET-70)	*m*-OH	I	*p*-OH	H	22 ± 2	111 ± 9	4

[a] EC_{50} is the half-maximal effective concentration of a compound.
[b] E_{max} is the maximum stimulation achieved at a concentration of 10 μM and was calculated by use of Prism software. EC_{50} and E_{max} values represent the average of N independent experiments in triplicate and were calculated by use of Prism software as described in the Experimental Procedures. The standard errors of the mean (SEM) were calculated from the EC_{50} and E_{max} values of each independent triplicate experiment by use of Prism software. E_{max} = 100% is defined as the activity of **1** at 10 μM.
[c] N is the number of independent experiments in triplicate that were performed and used to calculate the EC_{50} and E_{max} values.

Table 2. Agonist Activity of Compounds 14–26 on rTAAR$_1$

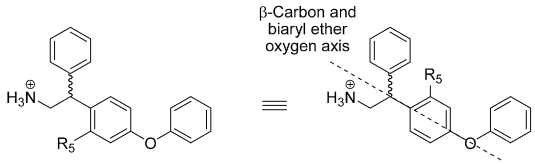

Compound	R_5	EC_{50}[a] ± SEM (nM)	E_{max}[b] ± SEM (%)	N[c]
14 (ET-51)	OH	96 ± 10	108 ± 1	3
15 (ET-52)	OMe	35 ± 4	82 ± 8	3
16 (ET-53)	OEt	144 ± 31	95 ± 5	3
17 (ET-54)	OPr	>1000	69 ± 5	2
18 (ET-55)	OBu	>1000	31 ± 1	2
19 (ET-56)	OBn	>1000	58 ± 2	2
20 (ET-57)	O-*i*Pr	>1000	62 ± 2	2
21 (ET-58)	O-*i*Bu	>1000	15 ± 4	2
22 (ET-59)	OCH_2CHCH_2	169 ± 6	71 ± 4	2
23 (ET-60)	OCH_2CCH	138 ± 37	78 ± 1	2
24 (ET-61)	$OCH_2CO_2CH_3$	>1000	56 ± 0	2
25 (ET-62)	$O_2CCH_2CH_2Cl$	143 ± 4	57 ± 5	2
26 (ET-63)	O_2CCH_3	234 ± 43	74 ± 3	2

[a] EC_{50} is the half-maximal effective concentration of a compound.
[b] E_{max} is the maximum stimulation achieved at a concentration of 10 μM and was calculated by use of Prism software. EC_{50} and E_{max} values represent the average of N independent experiments in triplicate and were calculated by use of Prism software as described in the Experimental Procedures. The standard errors of the mean (SEM) were calculated from the EC_{50} and E_{max} values of each independent triplicate experiment by use of Prism software. E_{max} = 100% is defined as the activity of **1** at 10 μM.
[c] N is the number of independent experiments in triplicate that were performed and used to calculate the EC_{50} and E_{max} values.

2 (E_{max} = 108% ± 1% and 95% ± 5%, respectively) but at ~3- to 5-fold lower potency (EC_{50} = 96 ± 10 nM and 144 ± 31 nM, respectively) (Table 2). By contrast, the methyl ether **15** showed the opposite trend, being equipotent to **2** (EC_{50} = 35 ± 4 nM) but less efficacious (E_{max} = 82% ± 8%). The unsaturated alkene and alkyne counterparts of the propyl ether **17** appear to be well tolerated by rTAAR$_1$, as **22** (EC_{50} = 169 ± 6 nM) and **23** (EC_{50} = 138 ± 37 nM) were at least 6-fold more potent than **17** (EC_{50} > 1 μM). The efficacies of **17**, **22**, and **23** were comparable to each other (E_{max} = 69% ± 5%, 71% ± 4%, and 78% ± 1%, respectively). Further increasing the size of the ether substituents (**18**–**21** and **24**) desirably decreased potency (EC_{50} > 1 μM) but did not completely abolish the agonist activity (E_{max} ≤ 10%) of the compounds. These compounds activated rTAAR$_1$ between 15% and 62% efficacy. Similarly, the ester substituents (**25** and **26**) decreased the potency of **2** (EC_{50} = 143 ± 4 nM and 234 ± 43 nM, respectively) but did not reduce its efficacy below 10% (E_{max} = 57% ± 5% and 74% ± 3%, respectively) (Table 2).

The observed agonist activities of **14**–**26** were consistent with the idea that the inner ring functional groups of these compounds were not properly interfering with the rotamer switch residues. In compound **14**, rotation of the inner ring about the β-carbon and the biaryl ether oxygen axis renders position 2 and 6 indistinguishable (Table 2). Within the binding site, it is possible that the inner rings of **15**–**26** have rotated 180° and are actually orienting the position 2 functional group toward the extracellular surface of rTAAR$_1$ around methionine 6.55 (M6.55) instead of the intracellular region near the rotamer switch residues. In this alternate binding orientation, these compounds would be

Figure 3. SAR of rTAAR$_1$ Ligands and Their Proposed Binding Mode in rTAAR$_1$
(A) Structure of **2**. The A, B, and C rings correspond to its outer, inner, and β-phenyl rings, respectively.
(B) Proposed binding orientation of **2** in the binding site of rTAAR$_1$, viewed from the perspective of TM4. The rotamer switch residues (white letters), proposed binding, and specificity determinant residues are labeled.
(C) Agonist dose-response curves of **2** (○), **27** (□), **29** (△), **34** (■), **50** (●), and **51** (▲). Dose-response curves were plotted and SEM were calculated from two or more independent triplicate experiments by use of Prism software.
(D) Proposed binding orientation of **34** in the binding site of rTAAR$_1$, viewed from the perspective of TM4.

Table 3. Agonist and Antagonist Activity of Compounds 27–49 on rTAAR$_1$

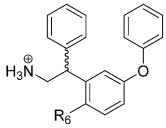

		Agonist Activity			Antagonist Activity		
Compound	R_6	EC_{50}[a] ± SEM (nM)	E_{max}[b] ± SEM (%)	N[c]	IC_{50}[d] ± SEM (μM)	I_{max}[e] ± SEM (%)	N[f]
27 (ET-14)	H	19 ± 2	131 ± 7	3	-	-	-
28 (ET-72)	OH	232 ± 8	88 ± 9	2	-	-	-
29 (ET-73)	OMe	102 ± 26	88 ± 1	3	-	-	-
30 (ET-74)	OEt	>1000	66 ± 3	2	-	-	-
31 (ET-75)	OPr	>1000	41 ± 0	2	-	-	-
32 (ET-76)	OBu	>1000	3 ± 0	2	8 ± 2	12 ± 3	2
33 (ET-77)	OPent	>1000	0 ± 3	2	5 ± 0	6 ± 1	2
34 (ET-78)	OHex	>1000	0 ± 1	2	4 ± 0	3 ± 1	4
35 (ET-79)	OBn	>1000	9 ± 1	2	5 ± 1	6 ± 3	2
36 (ET-80)	O-*i*Pr	>1000	40 ± 1	2	-	-	-
37 (ET-81)	O-*i*Bu	>1000	6 ± 1	2	>10	23 ± 6	2
38 (ET-82)	OCH_2CHCH_2	602 ± 10	79 ± 5	2	-	-	-
39 (ET-83)	OCH_2CCH	182 ± 46	103 ± 0	2	-	-	-
40 (ET-95)	OCH_2-cyclopropyl	>1000	26 ± 7	3	-	-	-
41 (ET-96)	OCH_2-cyclohexyl	>1000	0 ± 3	2	5 ± 1	9 ± 1	-
42 (ET-97)	$OCH_2CH_2CH_2CN$	>1000	3 ± 4	2	>10	30 ± 2	3
43 (ET-98)	$OCH_2CH_2CH_2CH_2CN$	>1000	2 ± 2	2	>10	23 ± 4	3
44 (ET-99)	OCH_2-(4-pyridinyl)	>1000	4 ± 2	2	7 ± 1	15 ± 2	3
45 (ET-100)	OCH_2-(3-pyridinyl)	>1000	9 ± 0	2	>10	33 ± 1	3
46 (ET-101)	OCH_2-(2-pyridinyl)	>1000	6 ± 1	2	7 ± 0	16 ± 2	3
47 (ET-84)	$O_2CCH_2CH_2Cl$	>1000	50 ± 8	2	-	-	-
48 (ET-85)	$O_2CCH(CH_3)_2$	599 ± 165	53 ± 6	2	-	-	-
49 (ET-86)	$O_2CCH_2CH(CH_3)_2$	>1000	33 ± 7	2	-	-	-

[a] EC_{50} is the half-maximal effective concentration of a compound.
[b] E_{max} is the maximum stimulation achieved at a concentration of 10 μM and was calculated by use of Prism software. EC_{50} and E_{max} values represent the average of N independent experiments in triplicate and were calculated by use of Prism software as described in the Experimental Procedures. The standard errors of the mean (SEM) were calculated from the EC_{50} and E_{max} values of each independent triplicate experiment by use of Prism software. E_{max} = 100% is defined as the activity of **1** at 10 μM.
[c] N is the number of independent experiments in triplicate that were performed and used to calculate the EC_{50} and E_{max} values.
[d] IC_{50} is the half-maximal inhibitory concentration of a compound at inhibiting the signal of fixed concentration of **1** (33 nM) in a competition assay.
[e] I_{max} is the maximum stimulation achieved by a fixed concentration of **1** (33 nM) when competed with a 10 μM dose of a compound. IC_{50} and I_{max} values represent the average of N independent experiments in triplicate and were calculated by use of Prism software as described in the Experimental Procedures. The standard errors of the mean (SEM) were calculated from the IC_{50} and I_{max} values of each independent triplicate experiment by use of Prism software. I_{max} = 100% is defined as the activity of **1** at 10 μM. I_{max} of T_1AM at 33 nM was 45% ± 5%.
[f] N is the number of independent experiments in triplicate that were performed and used to calculate the IC_{50} and I_{max} values.

predicted to have some agonist activity, as the ether or ester appendage would not be able to interfere with the rotamer switch residues.

To test this hypothesis, the core scaffold of **14** was modified to have the phenoxy group moved one carbon over to the *meta* position with respect to the ethylamine chain (**28**) (Table 3; Supplemental Scheme 7). In this orientation, the 2 and 6 positions of the inner ring are now structurally distinct. Having a *meta*-phenoxy group should not be detrimental to binding affinity because the isomer of **2** with the phenoxy group at the *meta* position (**27**) was found to be a slightly better agonist than **2** for rTAAR$_1$ (EC_{50} = 19 ± 2 nM, E_{max} = 131% ± 7%) (Figure 3C; Tan et al., 2007). With this modification, we synthesized 21 compounds (**29**–**49**) with an ether or ester appendage at the 2 position that again varied in steric bulk, rigidity, topology, and polarity (Table 3; Supplemental Schemes 7–9).

For the ether series (**29**–**46**), an interesting correlation was observed between the size of the position 2 substituent (R_6; Table 3) and the agonist activity of the compound. The core scaffold **28** was ~12-fold less potent (EC_{50} = 232 ± 8 nM) and 43% less efficacious (E_{max} = 88% ± 9%) compared to **27** (Table 3). Methylating the phenol of **28** (**29**) increased the potency ~2-fold (EC_{50} = 102 ± 26 nM) but had no effect on efficacy (E_{max} = 88% ± 1%). When the ether group was an ethyl ether or larger

Table 4. Agonist and Antagonist Activity of Compounds 50–56 on rTAAR$_1$

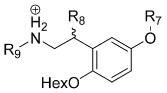

				Agonist Activity			Antagonist Activity		
Compound	R_7	R_8	R_9	EC_{50}[a] ± SEM (nM)	E_{max}[b] ± SEM (%)	N[c]	IC_{50}[d] ± SEM (μM)	I_{max}[e] ± SEM (%)	N[f]
50 (ET-88)	H	Ph	H	>1000	37 ± 9	2	-	-	-
51 (ET-89)	Ph	H	H	201 ± 23	59 ± 6	2	-	-	-
52 (ET-90)	Ph	Ph	CH_3	>1000	0 ± 3	2	5 ± 1	10 ± 4	3
53 (ET-91)	*p*-OH-Ph	Ph	H	>1000	16 ± 3	3	-	-	-
54 (ET-92)	*p*-F-Ph	Ph	H	>1000	0 ± 3	2	3 ± 0	0 ± 3	3
55 (ET-93)	*m*-F-Ph	Ph	H	>1000	0 ± 4	2	3 ± 1	0 ± 5	3
56 (ET-94)	*m*-CN-Ph	Ph	H	>1000	0 ± 4	2	3 ± 1	2 ± 4	3

[a] EC_{50} is the half-maximal effective concentration of a compound.
[b] E_{max} is the maximum stimulation achieved at a concentration of 10 μM and was calculated by use of Prism software. EC_{50} and E_{max} values represent the average of N independent experiments in triplicate and were calculated by use of Prism software as described in the Experimental Procedures. The standard errors of the mean (SEM) were calculated from the EC_{50} and E_{max} values of each independent triplicate experiment by use of Prism software. E_{max} = 100% is defined as the activity of **1** at 10 μM.
[c] N is the number of independent experiments in triplicate that were performed and used to calculate the EC_{50} and E_{max} values.
[d] IC_{50} is the half-maximal inhibitory concentration of a compound at inhibiting the signal of fixed concentration of **1** (33 nM) in a competition assay.
[e] I_{max} is the maximum stimulation achieved by a fixed concentration of **1** (33 nM) when competed with a 10 μM dose of a compound. IC_{50} and I_{max} values represent the average of N independent experiments in triplicate and were calculated by use of Prism software as described in the Experimental Procedures. The standard errors of the mean (SEM) were calculated from the IC_{50} and I_{max} values of each independent triplicate experiment by use of Prism software. I_{max} = 100% is defined as the activity of **1** at 10 μM. I_{max} of T_1AM at 33 nM was 45% ± 5%.
[f] N is the number of independent experiments in triplicate that were performed and used to calculate the IC_{50} and I_{max} values.

(**30**–**37**), the potency of the compound was poor (>1 μM). The efficacy showed a different profile. When the ether group was less than five atom units long (**30**, **31**, **36**, and **40**), the compound still had some degree of agonist activity (E_{max} = 26%–66%). As the ether group increased in size equal to or greater than five atom units long (**32**–**35** and **41**–**46**), the compounds became nonagonists, activating rTAAR$_1$ at less than 10% efficacy. An exception to this trend was **37**. Although its isobutoxy group is only four atom units long, **37** activated below 10% efficacy (E_{max} = 6% ± 1%). Compared to **31** (EC_{50} = >1 μM, E_{max} = 41% ± 0%), introducing an unsaturated alkene (**38**) or alkyne (**39**) into the position 2 group increased both potency (EC_{50} = 602 ± 10 nM and 182 ± 46 nM, respectively) and efficacy (E_{max} = 79% ± 5% and 103% ± 0%, respectively).

In the ester series (**47**–**49**), the potency of the compounds was greater than 1 μM when the position 2 functional group was five atom units long (**47** and **49**) but less than 1 μM when four atom units long (**48**, EC_{50} = 599 ± 165 nM) (Table 3). The efficacies of **47**–**49** were between 33% and 53%.

Because there are currently no binding assays available for rTAAR$_1$, the antagonist activity of the ten nonagonists (**32**–**35** and **41**–**46**) was determined by testing for the inhibition of cAMP production of rTAAR$_1$ in stably transfected HEK293 cells treated with EC_{50} concentration (33 nM) of **1**. Representative dose-response curves of antagonists against rTAAR$_1$ are shown in Figure S1B. This competition assay was validated in the β_2AR, where the antagonist propranolol was able to inhibit the cAMP production induced by the agonist isoproterenol (data not shown).

The ten nonagonists antagonized **1**-induced rTAAR$_1$ activation to varying degrees. The butyl ether **32** showed ca 75% antagonism with a half-maximal inhibitory concentration (IC_{50}) of 8 ± 2 μM (Table 3). Isobutyl ether **37** was also a weak antagonist, showing 50% inhibition and a potency of >10 μM. The longer pentyl and hexyl ethers (**33** and **34**, respectively) were better antagonists, reducing the **1** signal to 3%–6% at a potency of ~4–5 μM. The cyclohexylmethyl ether **41** was equally potent (IC_{50} = 5 ± 1 μM) but somewhat less inhibitory (I_{max} = 9% ± 1%). Compared to the benzyl ether **35** (IC_{50} = 5 ± 1 μM, I_{max} = 6% ± 3%), the heterocyclic pyridine methyl ethers (**44**–**46**) were less potent ($IC_{50} \geq 7$ μM) and inhibitory ($I_{max} \geq 15\%$). The cyanoalkyl ethers **42** and **43** were poor antagonists, inhibiting the **1** signal no lower than 23% with an IC_{50} value of >10 μM. The inhibitory effects of these compounds were neither due to inhibition of adenyl cyclase nor cytotoxicty (data not shown), suggesting that these compounds are bona fide rTAAR$_1$ antagonists.

Structure-Activity Relationship of rTAAR$_1$ Lead Antagonist

The agonist and antagonist properties of **27** and **34**, respectively, suggested that the hexyloxy group is essential for antagonism. To determine whether the outer ring (ring A in Figure 3A) and β-phenyl ring are also necessary for antagonism, we synthesized analogs of **34** lacking the outer ring (**50**) or the β-phenyl ring (**51**) (Table 4; Supplemental Schemes 10 and 11). In an attempt to improve the potency of **34**, we also explored the effects of N-methylation (**52**) and functionalization of the outer ring (**53**–**56**) (Table 4; Supplemental Schemes 8 and 10).

Removing the outer ring or β-phenyl ring of **34** was detrimental to rTAAR$_1$ antagonism. In the absence of the outer ring (**50**), **34** was converted into a weak agonist (Table 4; Figure 3C). Similarly, **34** became an agonist without the β-phenyl ring (**51**, EC_{50} = 201 ± 23 nM, EC_{50} = 59% ± 6%) (Figure 3C).

Mono-methylating the amine (**52**) or inserting electron-withdrawing groups on the outer ring (**54**–**56**) preserved the

antagonist activity of **34**. When screened for agonist activity, these compounds did not activate $rTAAR_1$ (Table 4). In the antagonist assay, the potency of **52** was unaffected (IC_{50} = 5 ± 1 μM) but the antagonist activity slightly decreased (IC_{50} = 10% ± 4%). The potency and inhibitory capacity of **34** was also not significantly affected by introducing a *para*-fluoro, *meta*-fluoro, or *meta*-cyano group into the outer ring (**54**, **55**, and **56**, respectively). The IC_{50} and I_{max} values of these compounds were ~3 μM and ≤2%, respectively. Interestingly, inserting a *para*-hydroxyl group into the outer ring (**53**) endowed some agonist activity to **34**, activating $rTAAR_1$ at >1 μM potency and 16% ± 3% efficacy.

DISCUSSION

The rotamer toggle switch model of aminergic GPCR activation (Figure 2) has proven to be a useful guideline in the design and synthesis of $rTAAR_1$ agonists and antagonists. Previous SAR studies on the ethylamine portion of **1** for $rTAAR_1$ provided **2** as a promising scaffold for developing $rTAAR1_1$ superagonists, which we define as compounds that are more potent and/or efficacious than **1** (Tan et al., 2007). In addition to being as potent and efficacious as **1**, **2** provides the added benefit of having many potential sites for derivatization. By analogy to the assumed binding mode of epinephrine to the β_2AR (Figure 1D), we deduced **2** to bind to $rTAAR_1$ in a similar fashion, with the charged amine forming a salt bridge interaction with D3.32 and the biaryl ether oxygen hydrogen bonding to S5.46 (Figure 3B). The β-phenyl ring is proposed to occupy a pocket near the interface of TM6 and TM7.

In the context of the rotamer toggle switch model, our analysis of the ligand-receptor interaction of β_2AR agonists showed that agonists generally lack functional groups in the region of the molecule that is predicted to be located in the vicinity of the rotamer switch residues. Structurally, most of these agonists appear to have functional groups that complement the physicochemical properties of the residues within the binding site. Following this lead, we attempted to improve the agonist properties of **2** by incorporating functional groups into the regions of the molecule (e.g., β-phenyl ring, charged amine, outer ring, and position 5 of the inner ring; Figures 3A and 3B) away from rotamer switch residues. In the β-phenyl ring, SAR studies presented here showed a clear preference for a hydroxyl group at the *para* position. The *para*-hydroxyl analog (**5**) was 24- to 78-fold and 8%–46% more potent and efficacious, respectively, compared to the *ortho*- or *meta*-hydroxyl analogs (**6** and **7**) and *ortho*- or *para*-methoxy (**3** and **4**) analogs. Additionally, the *para*-hydroxyl improved the potency and efficacy of **2** ~4.5-fold and 11%, respectively. We believe that this enhancement in agonist activity is a reflection of an increase in the binding affinity of **2** for $rTAAR_1$ due to hydrogen bond interactions of the *para*-hydroxyl with N7.39 and/or N7.35 (Figure 3B). Mutating residue 7.39 in the β_2AR has previously been found to perturb the binding affinity of agonists and antagonists (Suryanarayana et al., 1991). In the recently determined crystal structure of the β_2AR, N7.39 of the β_2AR was involved in hydrogen bond interactions with the β-carbon hydroxyl group of the partial inverse agonist carazolol (Cherezov et al., 2007; Rasmussen et al., 2007; Rosenbaum et al., 2007).

In the presence of the *para*-hydroxyl, mono-methylating the charged amine (**10**) or incorporating a **1** moiety into the molecule (**12**) was tolerated, but it had modest effects on agonist activity, if any at all. N-methyl **10** was equipotent to **5** but 13% more efficacious. By contrast, **12** essentially has the same potency and efficacy as **5**. The comparable levels of agonist activity of **5**, **10**, and **12** suggest that these compounds have similar interactions with $rTAAR_1$ and possibly elicit the same final active conformation of the receptor.

In contrast to the β_2AR agonists, our analysis of the SAR and potential binding modes of antagonists for the dopamine 1-like and 2-like receptors revealed the presence of structural moieties within these compounds that could conceivably sterically occlude the rotamer toggle switch residues from assuming their active conformation. Applying this hypothesis to $rTAAR_1$, we attempted to convert **2** into an antagonist by installing ethers and esters at the 2 position of the inner ring that varied in steric bulk, rigidity, topology, and polarity (**15**–**26**). Based on our proposed binding orientation of **2** (Figure 3B), this position was identified to be the prime location for presenting groups that could interfere with the rotamer switch residues in $rTAAR_1$. Unfortunately, none of these compounds turned out to be antagonists. Presumably, **15**–**26** were still able to activate $rTAAR_1$ between 15% and 95% efficacy, because the variable position 2 groups (R_5; Table 2) are positioned away from the rotamer switch residues within the binding site owing to rotation of the inner ring about the β-carbon and biaryl ether oxygen axis.

To circumvent this problem, we modified the core scaffold by moving the phenoxy group from the *para* (**14**) to the *meta* (**28**) position (Tables 2 and 3). With this modification, the agonist activity of the compound decreased as the size of the ether substituent increased (Figure 3C). When the ether group was ≥5 atom units long (**32**–**35** and **41**–**46**), the agonist activity of the compound was completely abolished (≤10% efficacy). Compounds with substituents less than five atom units long (**29**–**31**) were weak agonists, activating $rTAAR_1$ between 41% and 88% efficacy. The composition of the substituent appears to be important, as an ester group that is five atom units long (**47** and **49**) was still an agonist (EC_{50} = 33%–53%). When the nonagonists (**32**–**35** and **41**–**46**) were screened for antagonist activity in a competition assay with **1** at its EC_{50} concentration (33 nM), all compounds were found to inhibit **1**-induced cAMP production to varying degrees at 10 μM. Compound **34** was the best antagonist, showing >90% inhibition of $rTAAR_1$ activation with an IC_{50} value of 4 μM. The antagonist activities of **32**–**35** and **41**–**46** are thought to arise from the ether substituents sterically occluding F6.52 and/or W6.48 of the rotamer switch residues from assuming their active conformation.

The hexyloxy group, outer ring, and β-phenyl ring of **34** are all necessary for antagonism. In the absence of any one of these groups, the resulting compounds lose their antagonist activity and become agonists. Because the transformation of **34** to **27** yielded the greatest increase in agonist potency and efficacy, the hexyloxy group is the most important of the three structural elements in terms of decreasing agonist activity and conferring antagonist properties to **34** (Figure 3C). This is consistent with the notion that the outer ring and β-phenyl ring are essential scaffolding elements that assure **34** docks into the $rTAAR_1$ binding site in the proper orientation to position the hexyloxy group,

the molecular basis of antagonism, to interfere with the rotamer switch residues (Figure 3D).

SIGNIFICANCE

The rotamer toggle switch model of aminergic GPCR activation is a useful model for understanding the molecular basis of $rTAAR_1$ activation by 1 and related analogs. It has proven helpful in the development of $rTAAR_1$ agonists and antagonists, providing superagonists 5, 10, and 12 and lead antagonists 34, 54, and 55. This structure-activity relationship study suggests that agonist or antagonist properties of aminergic GPCR drugs could arise from probable drug interactions with the rotamer switch residues. Agonists allow the rotamer switch to toggle and/or have more favorable interactions with the active state of the receptor, whereas antagonists sterically occlude the rotamer switch and/or have more favorable interactions with the inactive state of the receptor.

These agonist and antagonist design principles have the potential to accelerate and increase the efficiency of the drug discovery and development process for GPCRs. Having insights into the critical ligand-receptor interactions important for receptor activation or inhibition facilitates the interpretation of SAR data and correlation of pharmacophore models with the molecular properties of the receptor binding site. This information then provides a map of the binding site landscape and presents a drug design blueprint for identifying promising scaffolds, recognizing compatible functional groups to incorporate, and evaluating the contribution of individual structural elements of a given compound toward its binding affinity, selectivity, and functional properties. We envision these principles to supplement all current GPCR drug design strategies (e.g., ligand-based drug design, focused library screening, virtual screening, structure-based drug design, etc.) (Evers and Klabunde, 2005; Evers et al., 2005; Klabunde and Evers, 2005; Klabunde and Hessler, 2002) and help generate predictive rules and guidelines that would prove to be a useful and general method for designing activators or inhibitors for biogenic amine GPCRs and possibly other rhodopsin-like GPCRs.

EXPERIMENTAL PROCEDURES

Residue Indexing System

Residues are labeled relative to the most conserved amino acid in the transmembrane segment in which it is located (Ballesteros and Weinstein, 1995). Tryptophan 6.48, for example, is located in transmembrane 6 and precedes the most conserved residue by 2 positions. Arginine 3.50 is the most conserved residue in TM3. This system simplifies the identification of corresponding residues in different GPCRs.

Homology Model of $rTAAR_1$

The sequence of $rTAAR_1$ was aligned to 26 human biogenic amine GPCRs (i.e., dopamine, α-adrenergic, β-adrenergic, and serotonin receptors) and the sequence for bovine rhodopsin (Protein Data Bank [PDB] code: 1F88) (Palczewski et al., 2000) using the program MUSCLE (Edgar, 2004). We constructed our homology model of $rTAAR_1$ based on the crystal structure of the inactive state bovine rhodopsin as a template and used our in-house software PLOP (commercially available as Prime from Schrödinger Incorporated). The modeling program did not modify conserved residues, leaving each atom in these residues at their original PDB coordinates. Nonconserved side chains were built onto the structure using the backbone coordinates for bovine rhodopsin as a reference point. All chain breaks or gaps were closed using a previously published loop building and optimization algorithm (Jacobson et al., 2004). After building the complete model, side-chain optimization, followed by backbone and side-chain energy minimization, was performed on all nonconserved residues. The homology modeling program relies on the OPLS all-atom force field (Jacobson et al., 2002; Jorgensen et al., 1996; Kaminski et al., 2001) and a generalized Born solvent model (Gallicchio et al., 2002; Ghosh et al., 1998) to evaluate the energy of different conformations and select the lowest-energy structure as the final model.

Synthesis

Detailed synthetic procedures and chemical compound information are described in the Supplemental Data.

In Vitro cAMP Assays: Agonist Activity Assay

After incubating in fresh medium for at least 2 hr, HEK293 cells stably transfected with $rTAAR_1$ were harvested in Krebs-Ringer-HEPES buffer (KRH) and preincubated with 200 μM 3-isobutyl-1-methylxanthine (IBMX) for 20–30 min. Cells were incubated in KRH with 133 μM IBMX and 3 μl of the test compound, forskolin (10 μM), or vehicle (dimethyl sulfoxide; DMSO) for 1 hr at 37°C (300 μl total volume). The cells were boiled for 20 min after addition of 100 μl of 0.5 mM sodium acetate buffer. The cell lysate was centrifuged to remove cellular debris, and an aliquot (30 μl) was transferred to an opaque, flat-bottom 96-well plate (Corning). The cAMP content of the aliquot was measured by use of the Hithunter cAMP XS kit (DiscoveRX). The plate was shaken on a titer plate shaker for 2 min after addition of 20 μl of cAMP XS antibody/lysis mix. After incubation in the dark for 1 hr, 20 μl of cAMP XS ED reagent was added and the plate was shaken for 2 min. After another hour of incubation in the dark, 40 μl of cAMP XS EA/CL substrate mix was added and the plate was shaken for 2 min. The plate was sealed with an acetate plate sealer (Thermo Scientific) and allowed to incubate in the dark for 15–18 hr before luminescence was measured (3 readings/well at 0.33 s/reading) on an Analyst AD assay detection system (LJL Biosystems) or a Packard Fusion microplate reader. Data were reported relative to **1** and expressed as % T_1AM. The activity of **1** at 10 μM was set as 100% T_1AM. Concentration-response curves were plotted and EC_{50} values were calculated with Prism software (GraphPad). Standard error of the mean was calculated from the EC_{50} and E_{Max} values of each independent triplicate experiment by use of Prism software.

In Vitro cAMP Assays: Antagonist Activity Assay

This was the same as the agonist activity assay procedure described above with the following changes: cells that were harvested in KRH buffer and preincubated with IBMX for 20–30 min were incubated in KRH with 133 μM IBMX and 3 μl of the putative antagonist or vehicle (DMSO) for 30 min at 37°C (300 μl total volume). Three microliters of the competing agonist (T_1AM, EC_{50} concentration [33 nM] as the final concentration), T_1AM (10 μM), forskolin (10 μM), or vehicle (DMSO) was then added to the reactions before incubating for 1 hr at 37°C. The cells were then processed as described in the agonist activity assay. Concentration-response curves were plotted and IC_{50} values were calculated with Prism software.

SUPPLEMENTAL DATA

Supplemental Data include one figure, eleven schemes, and Supplemental Experimental Procedures and can be found with this article online at http://www.chembiol.com/cgi/content/full/15/4/343/DC1/.

ACKNOWLEDGMENTS

This work was supported by grants from the National Institutes of Health (grant DK52798 to T.S.S.), Alfred P. Sloan Foundation (research fellowship to M.P.J.), and Ikaria, Incorporated. M.P.J. is a member of the Scientific Advisory Board of Shrödinger, Incorporated.

Received: December 5, 2007
Revised: February 5, 2008
Accepted: March 7, 2008
Published: April 18, 2008

REFERENCES

Ballesteros, J., and Weinstein, H. (1995). Integrated methods for the construction of three-dimensional models of structure-function relations in G protein-coupled receptors. Methods Neurosci. *25*, 366–428.

Ballesteros, J., Jensen, A., Liapakis, G., Rasmussen, S., Shi, L., Gether, U., and Javitch, J. (2001). Activation of the β(2)-adrenergic receptor involves disruption of an ionic lock between the cytoplasmic ends of transmembrane segments 3 and 6. J. Biol. Chem. *276*, 29171–29177.

Borowsky, B., Adham, N., Jones, K., Raddatz, R., Artymyshyn, R., Ogozalek, K., Durkin, M., Lakhlani, P., Bonini, J., Pathirana, S., et al. (2001). Trace amines: identification of a family of mammalian G protein-coupled receptors. Proc. Natl. Acad. Sci. USA *98*, 8966–8971.

Bunzow, J., Sonders, M., Arttamangkul, S., Harrison, L., Zhang, G., Quigley, D., Darland, T., Suchland, K., Pasumamula, S., Kennedy, J., et al. (2001). Amphetamine, 3,4-methylenedioxymethamphetamine, lysergic acid diethylamide, and metabolites of the catecholamine neurotransmitters are agonists of a rat trace amine receptor. Mol. Pharmacol. *60*, 1181–1188.

Cherezov, V., Rosenbaum, D.M., Hanson, M.A., Rasmussen, S.G., Thian, F.S., Kobilka, T.S., Choi, H.J., Kuhn, P., Weis, W.I., Kobilka, B.K., et al. (2007). High-resolution crystal structure of an engineered human β2-adrenergic G protein-coupled receptor. Science *318*, 1258–1265.

Edgar, R.C. (2004). MUSCLE: multiple sequence alignment with high accuracy and high throughput. Nucleic Acids Res. *32*, 1792–1797.

Evers, A., and Klabunde, T. (2005). Structure-based drug discovery using GPCR homology modeling: successful virtual screening for antagonists of the α1A adrenergic receptor. J. Med. Chem. *48*, 1088–1097.

Evers, A., Hessler, G., Matter, H., and Klabunde, T. (2005). Virtual screening of biogenic amine-binding G-protein coupled receptors: comparative evaluation of protein- and ligand-based virtual screening protocols. J. Med. Chem. *48*, 5448–5465.

Gallicchio, E., Zhang, L.Y., and Levy, R.M. (2002). The SGB/NP hydration free energy model based on the surface generalized Born solvent reaction field and novel nonpolar hydration free energy estimators. J. Comput. Chem. *23*, 517–529.

Gether, U. (2000). Uncovering molecular mechanisms involved in activation of G protein-coupled receptors. Endocr. Rev. *21*, 90–113.

Ghosh, A., Rapp, C., and Friesner, R. (1998). Generalized Born model based on a surface integral formulation. J. Phys. Chem. B *112*, 10983–10990.

Hart, M., Suchland, K., Miyakawa, M., Bunzow, J., Grandy, D., and Scanlan, T. (2006). Trace amine-associated receptor agonists: synthesis and evaluation of thyronamines and related analogues. J. Med. Chem. *49*, 1101–1112.

Jacobson, M., Kaminski, G., Friesner, R., and Rapp, C. (2002). Force field validation using protein side chain prediction. J. Phys. Chem. B *106*, 11673–11680.

Jacobson, M.P., Pincus, D.L., Rapp, C.S., Day, T.J., Honig, B., Shaw, D.E., and Friesner, R.A. (2004). A hierarchical approach to all-atom protein loop prediction. Proteins *55*, 351–367.

Jorgensen, W., Maxwell, D., and Tirado-Rives, J. (1996). Development and testing of the OPLS all-atom force field on conformational energetics and properties of organic liquids. J. Am. Chem. Soc. *118*, 11225–11236.

Kaminski, G., Friesner, R., Tirado-Rives, J., and Jorgensen, W. (2001). Evaluation and reparametrization of the OPLS-AA force field for proteins via comparison with accurate quantum chemical calculations on peptides. J. Phys. Chem. B *105*, 6474–6487.

Klabunde, T., and Evers, A. (2005). GPCR antitarget modeling: pharmacophore models for biogenic amine binding GPCRs to avoid GPCR-mediated side effects. ChemBioChem *6*, 876–889.

Klabunde, T., and Hessler, G. (2002). Drug design strategies for targeting G-protein-coupled receptors. ChemBioChem *3*, 929–944.

Kobilka, B., and Deupi, X. (2007). Conformational complexity of G-protein-coupled receptors. Trends Pharmacol. Sci. *28*, 397–406.

Liapakis, G., Ballesteros, J., Papachristou, S., Chan, W., Chen, X., and Javitch, J. (2000). The forgotten serine—a critical role for Ser-203(5.42) in ligand binding to and activation of the β(2)-adrenergic receptor. J. Biol. Chem. *275*, 37779–37788.

Liapakis, G., Chan, W., Papadokostaki, M., and Javitch, J. (2004). Synergistic contributions of the functional groups of epinephrine to its affinity and efficacy at the β(2) adrenergic receptor. Mol. Pharmacol. *65*, 1181–1190.

Lindemann, L., Ebeling, M., Kratochwil, N., Bunzow, J., Grandy, D., and Hoener, M. (2005). Trace amine-associated receptors form structurally and functionally distinct subfamilies of novel G protein-coupled receptors. Genomics *85*, 372–385.

Palczewski, K., Kumasaka, T., Hori, T., Behnke, C.A., Motoshima, H., Fox, B.A., Le Trong, I., Teller, D.C., Okada, T., Stenkamp, R.E., et al. (2000). Crystal structure of rhodopsin: a G protein-coupled receptor. Science *289*, 739–745.

Rasmussen, S.G., Choi, H.J., Rosenbaum, D.M., Kobilka, T.S., Thian, F.S., Edwards, P.C., Burghammer, M., Ratnala, V.R., Sanishvili, R., Fischetti, R.F., et al. (2007). Crystal structure of the human β2 adrenergic G-protein-coupled receptor. Nature *450*, 383–387.

Rosenbaum, D.M., Cherezov, V., Hanson, M.A., Rasmussen, S.G., Thian, F.S., Kobilka, T.S., Choi, H.J., Yao, X.J., Weis, W.I., Stevens, R.C., et al. (2007). GPCR engineering yields high-resolution structural insights into β2-adrenergic receptor function. Science *318*, 1266–1273.

Scanlan, T., Suchland, K., Hart, M., Chiellini, G., Huang, Y., Kruzich, P., Frascarelli, S., Crossley, D., Bunzow, J., Ronca-Testoni, S., et al. (2004). 3-iodothyronamine is an endogenous and rapid-acting derivative of thyroid hormone. Nat. Med. *10*, 638–642.

Shi, L., and Javitch, J. (2002). The binding site of aminergic G protein-coupled receptors: the transmembrane segments and second extracellular loop. Annu. Rev. Pharmacol. Toxicol. *42*, 437–467.

Shi, L., Liapakis, G., Xu, R., Guarnieri, F., Ballesteros, J., and Javitch, J. (2002). β(2) adrenergic receptor activation. Modulation of the proline kink in transmembrane 6 by a rotamer toggle switch. J. Biol. Chem. *277*, 40989–40996.

Snead, A.N., Santos, M.S., Seal, R.P., Miyakawa, M., Edwards, R.H., and Scanlan, T.S. (2007). Thyronamines inhibit plasma membrane and vesicular monoamine transport. ACS Chem. Biol. *2*, 390–398.

Strader, C., Sigal, I., Candelore, M., Rands, E., Hill, W., and Dixon, R. (1988). Conserved aspartic-acid residue-79 and residue-113 of the β-adrenergic-receptor have different roles in receptor function. J. Biol. Chem. *263*, 10267–10271.

Strader, C., Candelore, M., Hill, W., Sigal, I., and Dixon, R. (1989a). Identification of two serine residues involved in agonist activation of the β-adrenergic-receptor. J. Biol. Chem. *264*, 13572–13578.

Strader, C., Sigal, I., and Dixon, R. (1989b). Structural basis of β-adrenergic-receptor function. FASEB J. *3*, 1825–1832.

Strader, C., Fong, T., Tota, M., Underwood, D., and Dixon, R. (1994). Structure and function of G-protein coupled receptors. Annu. Rev. Biochem. *63*, 101–132.

Suryanarayana, S., Daunt, D., von Zastrow, M., and Kobilka, B. (1991). A point mutation in the seventh hydrophobic domain of the α-2-adrenergic-receptor increases its affinity for a family of β-receptor-antagonists. J. Biol. Chem. *266*, 15488–15492.

Swaminath, G., Xiang, Y., Lee, T., Steenhuis, J., Parnot, C., and Kobilka, B. (2004). Sequential binding of agonists to the β(2) adrenoceptor—kinetic evidence for intermediate conformational states. J. Biol. Chem. *279*, 686–691.

Tan, E., Miyakawa, M., Bunzow, J., Grandy, D., and Scanlan, T. (2007). Exploring the structure-activity relationship of the ethylamine portion of 3-iodothyronamine for rat and mouse trace amine-associated receptor 1. J. Med. Chem. *50*, 2787–2798.

Tota, M.R., Candelore, M.R., Dixon, R.A., and Strader, C.D. (1991). Biophysical and genetic analysis of the ligand-binding site of the β-adrenoceptor. Trends Pharmacol. Sci. *12*, 4–6.

Wainscott, D., Little, S., Yin, T., Tu, Y., Rocco, V., He, J., and Nelson, D. (2007). Pharmacologic characterization of the cloned human trace amine-associated receptor1 (TAAR1) and evidence for species differences with the rat TAAR1. J. Pharmacol. Exp. Ther. *320*, 475–485.

Wess, J. (1998). Molecular basis of receptor/G-protein-coupling selectivity. Pharmacol. Ther. *80*, 231–264.

Wieland, K., Zuurmond, H., Krasel, C., Ijzerman, A., and Lohse, M. (1996). Involvement of Asn-293 in stereospecific agonist recognition and in activation of the β(2)-adrenergic receptor. Proc. Natl. Acad. Sci. USA *93*, 9276–9281.

Yao, X., Parnot, C., Deupi, X., Ratnala, V., Swaminath, G., Farrens, D., and Kobilka, B. (2006). Coupling ligand structure to specific conformational switches in the β(2)-adrenoceptor. Nat. Chem. Biol. *2*, 417–422.

Zucchi, R., Chiellini, G., Scanlan, T., and Grandy, D. (2006). Trace amine-associated receptors and their ligands. Br. J. Pharmacol. *149*, 967–978.

Zuurmond, H., Hessling, J., Bluml, K., Lohse, M., and Ijzerman, A. (1999). Study of interaction between agonists and Asn293 in helix VI of human β(2)-adrenergic receptor. Mol. Pharmacol. *56*, 909–916.

